Modelling and control of handling dynamics for a hydrostatically driven vehicle

Justin Sill, Sisay Molla and Beshah Ayalew*

Clemson University International Center for Automotive Research,
4 Research Dr., 342 CGEC,
Greenville, SC 29607, USA
E-mail: jsill@clemson.edu,
E-mail: smolla@clemson.edu
E-mail: beshah@clemson.edu
*Corresponding author

Abstract: This paper presents a model for analysing the handling dynamics and lateral stability control of a vehicle featuring a hydrostatic independent wheel drive system for integrating energy efficiency with safety. The stability control system determines the necessary corrective yaw moment and achieves correction of oversteer or understeer via a controlled differential actuation of the wheel-end hydraulic pump/motors. During aggressive handling manoeuvres, the motors can be operated as pumps for re-generating the vehicle's kinetic energy into on-board hydraulic accumulators. This system has the distinct benefit of avoiding excessive activation of the friction brakes as is common in current stability control technology.

Keywords: hydrostatic drives; hydraulic hybrid vehicle; handling stability control; accumulators; hydraulic pumps and motors; independent drive.

Biographical notes: Justin Sill is a PhD candidate in Automotive Engineering at the Clemson University's International Center for Automotive Research. He earned Masters and Bachelors Degrees in Mechanical Engineering from Clemson University in South Carolina. He was also a Research Assistant and a Graduate Teaching Assistant at Clemson. He then worked at Goodyear Tyre Company as a Vehicle Dynamics Engineer for more than three years before returning to graduate school for his doctoral work. His research interests and expertise are in modelling and control of dynamic systems, and track testing and modelling of vehicle/tyre performance. He is a member of ASME and SAE.

Sisay Molla received his Bachelors Degree in Mechanical Engineering from Addis Ababa University, Addis Ababa, Ethiopia, in 2006. He then worked as an Assistant Lecturer at the same university until July 2008. He subsequently earned his Masters Degree, also in Mechanical Engineering, from Clemson University in 2010. His research interests include hybrid vehicle powertrain system modelling, dynamic system modelling and control, optimal control of vehicular and energy systems, fluid power systems. He is a member of the SAE.

Beshah Ayalew is currently an Assistant Professor at Clemson University-International Center for Automotive Research. He earned his BS Degree from Addis Ababa University (1997) and his MS (2000) and PhD Degrees (2005) from the Pennsylvania State University, all in Mechanical Engineering. Before joining Clemson, he was a Research Associate at the Pennsylvania Transportation Institute. He was a Fellow of the US DOE's GATE program and was awarded the 2005 Penn State Alumni Association Dissertation Award. His research interests are in dynamic systems and control, fluid power systems and robotics. He is a member of ASME, SAE and IEEE.

1   Introduction

Growing concerns about increasing pollution and resource depletion have accelerated the development of alternative vehicle propulsion systems that emphasise energy efficiency. Some of the many proposed such systems are variants of hydrostatic (hydraulic hybrid) drives. Hydraulic hybrids have been shown to significantly improve fuel efficiency over conventional drive trains, particularly for heavy urban vehicles that feature frequent stop and go motion (Buchwald et al., 1979; Kargul, 2006; Wu et al., 2004). In addition, the high specific-power (peak power per unit mass) of hydrostatic components opens up the possibility of using multiple but smaller P/M for a per-axle or a per-wheel drive arrangement.

Vehicle Stability Control (VSC) systems help reduce accidents by minimising driver's loss of control of the vehicle during emergency or aggressive manoeuvres. Central to these VSC systems is the generation of a corrective vehicle yaw moment through control of the longitudinal forces on select tyres of the vehicle. Most VSC systems available on the market today are brake-based and mainly extend the functionality of mature hardware technology available for anti-lock braking systems. These VSC systems facilitate differential (left-to-right) braking to generate the required corrective or stabilising yaw moment (VanZanten, 2000; Ghoneim et al., 2000; Rajamani, 2006). However, this strategy slows the vehicle against driver intent and leads to energy waste through heat and wear of the friction brakes. An alternative approach for generating the corrective yaw moment that avoids the drawbacks of the brake-based strategies is to distribute the tractive/braking force differentially between driving wheels (Esmailzadeh et al., 2002; Goodarzi and Esmailzadeh, 2007; Karogal and Ayalew, 2009; Osborn and Shim, 2004). Current solutions based on this strategy include the so-called torque-vectoring systems which employ active differentials within conventional powertrains (Piyabongkarn et al., 2007; Gradu, 2003).

In this paper, an independent hydrostatic drive system is considered where the traction/braking force of each wheel is controlled by modulating the torque output of individual wheel motors. This arrangement is a type of a series hydraulic hybrid powertrain. The goal is to exploit the arrangement and integrate both the demonstrated energy efficiency benefits of hydraulic hybrids and the safety of VSC. Even though the discussion focuses on independent hydrostatic drives, the integrative consideration of energy efficiency and stability control addressed here can be broadened to similar independent wheel drives for series electric hybrids, pure electric, and fuel cell vehicles.

The schematic of the proposed system is shown in Figure 1. It includes an Internal Combustion Engine (ICE) driven pump, accumulators, and four individual wheel-end

P/M. The ICE is directly connected to the pump which converts the mechanical power of the engine to hydraulic power. The fluid from the pump either charges the high pressure accumulator or directly flows to the individual wheel-end P/M. The ICE can be turned off to improve system efficiency when the vehicle comes to a full stop or when the State of Charge (SOC) of the accumulator is greater than a minimum threshold. The wheel-end P/Ms can be operated either as motors in drive mode or pumps during regenerative braking and/or when the VSC dictates it.

Figure 1   Schematic of a 4 × 4 independent hydrostatic wheel drive system (see online version for colours)
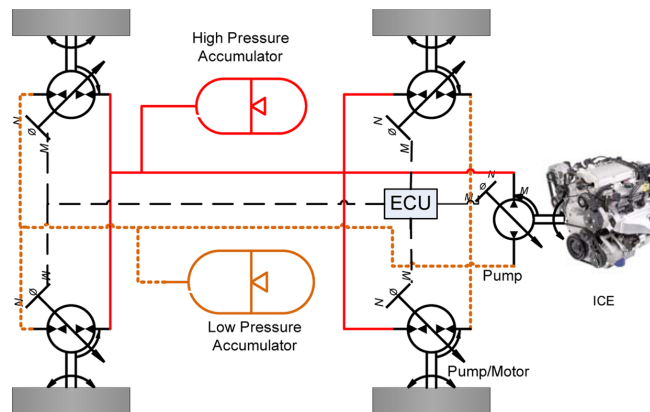
For the analysis in this work, a model of a 4 × 4 hydrostatic independent wheel drive system is assembled in a causal and modular fashion and is coupled to a 7 Degree of Freedom (DOF) vehicle handling dynamics model. The integrated system model is then used to first verify component selection and hybrid control threshold settings for the independent hydrostatic drive system. Then, a vehicle handling stability control system is established as a cascade of yaw rate feedback control and torque distribution schemes. A nominally oversteering vehicle is considered and the performance of the VSC system in improving the handling potential is evaluated. The combined stability control and energy recovery attributes of the independent drive system are shown using simulations of aggressive accident avoidance type handling manoeuvres.

The rest of the paper is organised as follows. Section 2 presents the details of the component and system models and their causal interconnections. Section 3 outlines the control strategies for the powertrain and VSC using the proposed drive system. In Section 4, the developed models are used to demonstrate the potential of the proposed system for enhancing VSC while recovering energy. Finally, in Section 5, the conclusions and possible future research directions are summarised.

2   System modelling

The high-level system model architecture comprises the engine and hydrostatic powertrain subsystems, the supervisory controller, the driver and vehicle dynamics subsystems as depicted in Figure 2. The individual components of each of these subsystems are developed on the basis of forward-facing models interconnected

by enforcing strict physical causality. The adopted causal interconnections between the subsystems are shown in Figure 3. Here, the accumulator pressure is an output of the accumulator model (which may or may not include an inlet orifice). The accumulator pressure is then enforced on the junction, and subsequently on the wheel-end P/M and the engine side pump. Likewise, the vehicle speed dictates the P/M speed and subsequently the flow rate into the junction from the P/M unit. The junction is a summing point for the flow rates into/from the accumulator, the engine side pump and the wheel-end P/M. The details of each of the component models are outlined in the following subsections.

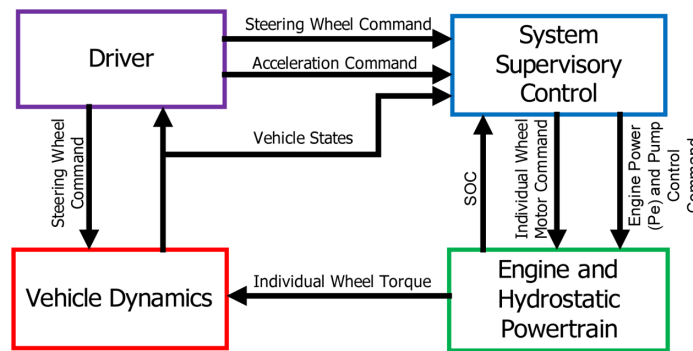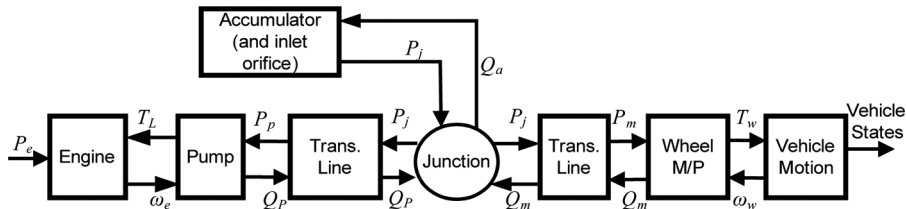**Figure 2** High-level system model architecture (see online version for colours)

Figure 3 Causal interconnection of hydrostatic powertrain component models

2.1 Hydrostatic powertrain

The model of the hydrostatic powertrain subsystem includes derived models for the pump/motor, accumulator, reservoir (low pressure accumulator) and hydraulic transmission lines.

2.1.1 Pump/Motor model

The four P/Ms considered are of the bent-axis design and are mechanically coupled to the wheels of the vehicle through a speed-reducing gearbox. The P/M units convert available hydraulic power from the engine-driven pump or the accumulator into mechanical power for vehicle propulsion (in motor mode), or convert the kinetic energy of the vehicle into hydraulic energy for storage in the accumulator during regenerative braking (in pump mode). Either the motor or pump mode can be activated for the P/M units individually to generate a prescribed corrective yaw moment for VSC.

The P/M units are modelled here based on 3-D look-up tables of measured steady-state efficiency data. This look-up table approach avoids the need for the numerous dimensionless numbers and loss coefficients frequently used in pump/ motor modelling following Wilson's pump theory (McCandlish and Dorey, 1984; Wilson, 1946). The torque and the flow rate through the variable displacement P/M are functions of, and can be controlled by, the displacement factor, *x*, which is defined as the ratio of the prevailing displacement to the maximum displacement of the machine. The relationship given by the look-up tables are denoted as functions $\eta(x, \omega, \Delta P)$ where the arguments (inputs) are *x*, ω, and ΔP across the P/M unit and the volumetric efficiency η_v and the mechanical efficiency η_m of the P/M unit are interpolated for as outputs. Knowing these efficiency values, the flow rate and the torque of the P/M can be computed by using the following sets of equations which also define the causal-relationships adopted for the P/M unit (McCandlish and Dorey, 1984; Pease and Henderson, 1988; Pourmovahed, 1991).

$$Q = x \cdot \omega \cdot D \cdot \eta_v^{\pm 1}(x, \omega, \Delta P) \tag{1}$$

$$T_a = \frac{x \Delta P D}{\eta_m^{\mp 1}(x, \omega, \Delta p)} \tag{2}$$

where the $\pm$ signs on the superscripts correspond to the pump (+) or motor (–) modes of operations for the P/M unit under consideration. This is verified by the fact that for a pump the actual flow rate is actually lower than the ideal volumetric flow rate due to leakage and fluid compressibility. On the other hand, the actual torque required to operate the pump is greater than the ideal one (determined by the differential pressure across the machine and its displacement) due to inevitable frictional losses. The opposite is true in the case of motor mode of operation for the P/M unit.

The rotational speed dynamics for the wheel-end motors is coupled with the vehicle dynamics through the tyre-wheel dynamics, a gear reduction and a driver model (see equation (18), and following discussion).

2.1.2 *Accumulator/reservoir model*

An accumulator is a pressure vessel that contains a hydraulic fluid and a pressurised inert gas (commonly nitrogen) where the two sides are separated by a bladder, a diaphragm or a piston. When hydraulic fluid is pumped in, the gas is compressed, causing the pressure to increase and store energy. When the fluid is discharged through the P/M (in motor mode), the pressure in the gas decreases while delivering propulsion energy. A reservoir (or low pressure accumulator) is a hydraulic accumulator working at much lower pressure just enough to prevent the occurrence of cavitation in the P/M units.

Considering the use of elastomeric foam on the gas side of the accumulator (to reduce irreversible heat losses) and taking energy balance on the gas side, it can be shown that the temperature evolution is given by Pourmovahed et al. (1992) and Pourmovahed (1990):

$$\left[1 + \frac{m_f c_f}{m_g c_v}\right] \frac{dT}{dt} = \frac{T_w - T}{\tau} - \frac{T}{C_v}\left(\frac{\partial p_g}{\partial T}\right)_v \frac{dv}{dt} \tag{3}$$

where τ is the average thermal time constant, which is defined as $\tau = m_g c_v / h A_w$, with an average effective wall area, A_w, and convective heat transfer coefficient, h. The pressure in the accumulator is related to the gas temperature and the specific volume through a real-gas equation of state, such as the Beattie-Bridgeman (BB) equation of state (Cengel and Boles, 2005):

$$p_g = \frac{RT(1-\varepsilon)}{v^2} + (v+B) - A/v^2 \tag{4}$$

where, $A = A_0(1 - a/v)$, $B = B_0(1-b)/v$, $\varepsilon = c/(vT^3)$ and A_0, B_0, a, b, c are constants in the BB equation of state. The specific volume of the gas is related to the accumulator flow rate (Q_{acc}) as:

$$\frac{dv}{dt} = \frac{-Q_{acc}}{m_g} \tag{5}$$

with,

$$
\begin{aligned}
Q_{acc} &= \sum_{i=1}^{n} Q_{p/m,i} + Q_p \\
&= \sum_{i=1}^{n}\left[x_{p/m,i} D_{p/m,i} \omega_{p/m,i} \eta_{v,i}^{\pm 1}(x_{p/m,i}, \omega_{p/m,i}, \Delta p_{p/m,i}) \right] \\
&\quad + x_p D_p \omega_p \eta_v(x_p, \omega_p, \Delta p_p).
\end{aligned}
\tag{6}
$$

The first term on the right side of equation (6) is the sum of the flow rate to/from the individual wheel-end P/Ms ($i = 1 : n$), considered positive in pump mode. And the second term is the flow rate from the engine-driven pump, also positive in pump mode. The hydraulic fluid flow rate into the accumulator (charging) is taken as positive. The State of Charge (SOC) of the accumulator is defined as the ratio of the instantaneous oil volume in the accumulator to the maximum possible oil capacity and is given by:

$$
\begin{aligned}
SOC &= \frac{\int_{V_0}^{V} Q_{acc} dt}{V_{acc}} \\
&= \frac{\int_{V_0}^{V} \left(\sum_{i=1}^{n}\left[x_{p/m,i} D_{p/m,i} \omega_{p/m,i} \eta_{v,i}^{\pm 1}(x_{p/m,i}, \omega_{p/m,i}, \Delta p_{p/m,i}) \right] + x_p D_p \omega_p \eta_v(x_p, \omega_p, \Delta p_p) \right) dt}{V_{acc}}.
\end{aligned}
\tag{7}
$$

However, measuring the instantaneous oil volume is not straightforward for the purposes of hydrostatic system control. As long as the temperature variation in the accumulator is kept low, the more directly measurable fluid/gas pressure can be used as an indicator of the SOC of the accumulator provided appropriate margins are considered (Kim and Filipi, 2007). The SOC can be estimated from the gas pressure as follows:

$$SOC = \frac{P_g - P_l}{P_{max} - P_l} \tag{8}$$

where P_l is the lower pressure limit of the accumulator corresponding to what is taken to be a zero SOC.

2.1.3 Hydraulic transmission lines

In the present application, the dynamic effects in the transmission lines (including compliance of the fluid and flexible hoses and the line inertances) are considered negligible in the present applications since the relevant frequencies are rather low (<10 Hz or so). This makes it possible to use a one-dimensional lumped parameter resistive model for the transmission lines instead of more elaborate dynamic and distributed parameter models (Watton, 1989; Ayalew and Kulakowski, 2005). The resistive pressure drop along transmission lines and fittings can be expressed mathematically as a function of the Reynolds number (Pourmovahed et al., 1992):

$$\Delta P_f = P_1 - P_2 = f(R_e)\frac{L\rho Q^2}{2D_p A^2} \tag{9}$$

where, L is the total effective length of the transmission line between two components (indexed 1, and 2), ρ as the fluid density, Q as the flow rate through the pipe/hose, D_p is the internal diameter of the pipe, and A as the cross sectional area of the pipe. The friction coefficient f is given by:

$$f = \begin{cases} 64/\text{Re} & \text{Re} \leq 2000, & \text{laminar flow} \\ 0.332\,\text{Re}^{-1/4} & 2000 < \text{Re} < 10000, & \text{turbulent flow} \end{cases} \tag{10}$$

where Re is the Reynolds number and is defined by

$$\text{Re} = \frac{4Q}{\pi D_p \nu}$$

where, ν is the kinematic viscosity of the fluid. Combining the above equations, the high pressure side of the motor or pump, i.e., the motor inlet pressure and the pump discharge pressure, are given by:

$$P_{m,p} = P_j + \text{sgn}(Q)\Delta P_f. \tag{11}$$

The junction pressure P_j is related to the gas pressure P_g considering the accumulator flow rate through the inlet orifice.

$$P_j = P_g + \text{sgn}(Q_{acc})Q_{\text{acc}}^2 K \tag{12}$$

where

$$K = \frac{\rho}{2(C_d A_{\text{orifice}})^2}$$

contains the orifice parameters: the discharge coefficient C_d and its area A_{orifice}.

2.2 Engine-pump subsystem

The model of the engine subsystem is also implemented as quasi-steady state model, combining the dynamics of the engine-pump rotational inertia with the fuel consumption map of the engine. It is first assumed that engine power (P_e) is determined by the power management strategy (described below) in the supervisory system controller. Given the power P_e, one can read-off the desired engine torque T_e and desired engine speed ω_{e_des}, corresponding to the minimum Brake Specific Fuel Consumption (BSFC) line of the engine at that power level. Neglecting torque generation delays, it is assumed here that the actual engine torque matches the desired. Then, the actual speed of the engine-pump ($\omega_{e/p}$) is determined from the rotational dynamics:

$$J_{eq}\dot{\omega}_{e/p} = T_e - T_L(x_p, \omega_p, \Delta P_p) \tag{13}$$

where T_L is the load torque (pump torque) on the engine, and $J_{eq.}$ is the equivalent engine-pump rotational inertia. The actual speed of the engine/pump from equation (13) is controlled via the displacement of the pump (through its displacement factor x_p) to track the desired engine speed, ω_{e_des}, which is selected based on the minimum BSFC speed of the engine at the current power level. A PI controller is used to minimise the speed error from this value:

$$x_p = k_p(\omega_{e\_des} - \omega_{e/p}) + K_i \int (\omega_{e\_des} - \omega_{e/p}) \cdot dt. \tag{14}$$

Here, k_p and k_i are the proportional and integral gains. Note that the displacement factor x influences the pump torque via equation (2) and eventually the engine speed via equation (13).

2.3 Vehicle dynamics model integration

The above models of the hydrostatic powertrain and the engine-pump subsystems are integrated with a 7-DOF handling dynamics model. The handling model includes the degrees of freedom of lateral and longitudinal motions yaw rotation, and the rotations of the four tyres. This model ignores suspension effects and therefore does not consider the pitch, heave, and roll of the vehicle body. Detailed derivations and discussions of the model are given in Genta (1997), Karogal and Ayalew (2009) and Osborn and Shim (2004). The longitudinal, lateral, and yaw equations of motion are:
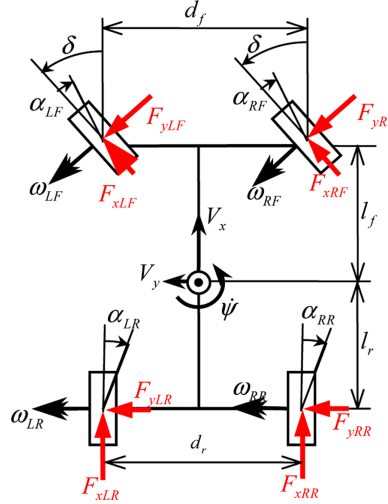
$$m(\dot{V}_x - V_y\dot{\psi}) = \sum F_x = (F_{xLF} + F_{xRF})\cos(\delta) - (F_{yLF} + F_{yRF})\sin(\delta)$$
$$+ F_{xLR} + F_{xRR} - \frac{1}{2}\rho C_D A V_x^2 - mgC_{RR} \tag{15}$$

$$m(\dot{V}_y + V_x\dot{\psi}) = \sum F_y = (F_{yLF} + F_{yRF})\cos(\delta)$$
$$+ (F_{xLF} + F_{xRF})\sin(\delta) + F_{yLR} + F_{yRR} \tag{16}$$

$$I_{zz}\ddot{\psi} = \sum M_z = l_f\left[(F_{yLF} + F_{yRF})\cos(\delta) + (F_{xRF} + F_{xLF})\sin(\delta)\right] - l_r(F_{yLR} + F_{yRR})$$
$$+ \frac{d_f}{2}\left[(F_{xRF} - F_{xLF})\cos(\delta) + (F_{yLF} - F_{yRF})\sin(\delta)\right] + \frac{d_r}{2}(F_{xRR} - F_{xLR}). \tag{17}$$

The notations used in equations (15)–(17) are defined in Figure 4 and in the nomenclature list.

Figure 4   Schematic of vehicle dynamics model (see online version for colours)

The tyre/wheel dynamics connect the hydraulic wheel-end P/M torque to the dynamics of the vehicle via the longitudinal tyre forces. The tyre/wheel dynamics are given by:

$$I_w \dot{\omega}_i = T_{w,i} - F_{x,i} R_w \quad \text{for } i = \text{LF}, \text{RF}, \text{LR}, \text{RR} \tag{18}$$

where LF, RF, LR and RR stand for left front, right front, left rear, and right rear tyres.

Each wheel torque and speed is related to the wheel-end motor torque and speed via a fixed gear-reduction ratio. The motor torque $T_{p,m}$ is determined from equation (2), where the displacement factor of each respective motor is determined from a vehicle speed controller (or driver model, which is a *P* or PI type controller similar to equation (14)) and/or the vehicle stability controller described in the next section. The motor torques $T_{p/m}$ will be substituted by the friction brake torques when regenerative braking alone would not give the desired level of deceleration and when the accumulator is fully charged.

The tyre forces are determined by the operating conditions for each tyre, specifically, normal loads, longitudinal slip ratios, and lateral slip angles. Considering the load transfers that occur due to lateral and longitudinal accelerations and differences in the front and rear roll-stiffness distributions, the prevailing tyre normal loads can be computed within the simplified 7 DOF model described above. The loads for the LF and LR tyres are given by (others follow similarly):

$$F_{\text{LF}} = \frac{mgl_r}{2L} - \left(\dot{V}_y + V_x\dot{\psi}\right)\left(\frac{ml_r h_{rcF}}{Ld_f} + \frac{m(h_{cg} - h_{rcF})K_{\phi F}}{d_f(K_{\phi F} + K_{\phi R} - mg(h_{cg} - h_{rcF}))}\right) - \left(\dot{V}_x - V_y\dot{\psi}\right)\left(\frac{mh_{cg}}{2L}\right)$$

$$F_{\text{LR}} = \frac{mgl_f}{2L} - \left(\dot{V}_y + V_x\dot{\psi}\right)\left(\frac{ml_f h_{rcR}}{Ld_r} + \frac{m(h_{cg} - h_{rcR})K_{\phi R}}{d_r(K_{\phi F} + K_{\phi R} - mg(h_{cg} - h_{rcR}))}\right) + \left(\dot{V}_x - V_y\dot{\psi}\right)\left(\frac{mh_{cg}}{2L}\right).$$

$$\tag{19}$$

The tyre slip ratios and slip angles are computed from the vehicle's longitudinal and lateral velocities, yaw rate, wheel spin and steer angle as:

$$\kappa_i = \frac{\omega_i R_w}{V_{xi}} - 1 \quad \text{for } i = \text{LF, RF, LR, RR} \tag{20}$$

$$\alpha_{\text{LF}} = \tan^{-1}\left(\frac{V_y + l_f\dot{\psi}}{V_x + \frac{d_f}{2}\dot{\psi}}\right) - \delta, \quad \text{and, } \alpha_{LR} = \tan^{-1}\left(\frac{V_y - l_r\dot{\psi}}{V_x + \frac{d_r}{2}\dot{\psi}}\right). \tag{21}$$

Since longitudinal tractive forces are to be exploited to influence the lateral handling dynamics with the present hydrostatic system, a proper tyre model that considers combined slip conditions (longitudinal and lateral) must be used, i.e., models that give $F_x = F_x(\kappa, \alpha, F_z)$ and $F_y = F_y(\kappa, \alpha, F_z)$ are needed. In combined slip conditions, when the longitudinal slip ratio approaches its extreme values ($\kappa = -1$ or ∞) there is no lateral force capacity. Conversely, when the lateral slip angle α becomes extreme, the longitudinal force capacity reduces to small values. In the present work, combined slip tyre data provided in Pacejka (2002) have been suitably scaled and implemented as a multi-dimensional lookup table.

3 Supervisory control

The supervisory control is the top level control where the command for engine power, the commands for individual wheel torque (via the displacement factors), and the command for supplementary friction brake activation are determined to meet the vehicle safety and energy efficiency objectives. As shown in Figure 2, the supervisory controller takes the vehicle states (longitudinal and lateral speeds, yaw rate, and rotational speed of individual wheels), the steering wheel angle and acceleration/braking signals, and the SOC of the accumulator as input commands from the sub-models of vehicle dynamics, driver and hydrostatic powertrain, respectively. It then determines the individual wheel torques, the engine power and friction brake activation commands for the hydrostatic and vehicle dynamics subsystems.

3.1 Power management strategy

A power management strategy is needed to determine the split between the two power sources (the engine-pump set or the accumulator) in such a way as to minimise fuel consumption and reduce emissions. Different energy management strategies have been discussed in the literature on hybrid vehicles (Brahma et al., 2000; Jalil et al., 1997; Kim and Filipi, 2007; Lin et al., 2003; Filipi et al., 2004). In the present work, a robust, yet simple management strategy is adopted from Kim and Filipi (2007) and is shown in Figure 5.

Figure 5   Schematic representation of engine power as a function accumulator SOC
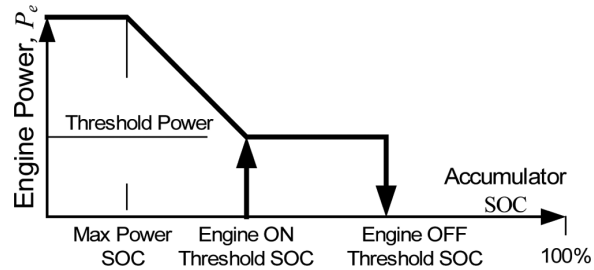
In this strategy, the engine power command (P_e) increases or decreases progressively based on the SOC of the accumulator. As long as the SOC is above engine-off threshold value, say 40%, the engine power command is set to zero, and the drive power is supplied entirely from the accumulator. When the SOC of the accumulator drops below the threshold value, the engine starts charging the accumulator and/or contributing to the drive power, while running at pre-determined threshold power command (say 45 kW, for this work). An SOC dead band of 10% or so is taken to avoid frequent engine on-off cycling. If the power demand is such that it exceeds the engine threshold power and the SOC drops below the engine-on threshold SOC of the dead band (say 30%) and the engine power command is progressively increased along the minimum BSFC line on the torque-speed map of the engine. With further increase in propulsion power demand, the powertrain works in a hydrostatic Continuously Variable Transmission (CVT) mode, with the engine operating at a maximum power trying to keep the SOC of the accumulator above a minimum (Max Power SOC, say 10%).

The other function of supervisory control is the activation of supplementary friction brakes. If the vehicle needs to decelerate further while the SOC of the accumulator indicates full (accumulator reaches maximum pressure) or if the torque available from the hydraulic system is not enough for braking, then the friction brakes need to be activated to bring the vehicle to the desired speed.
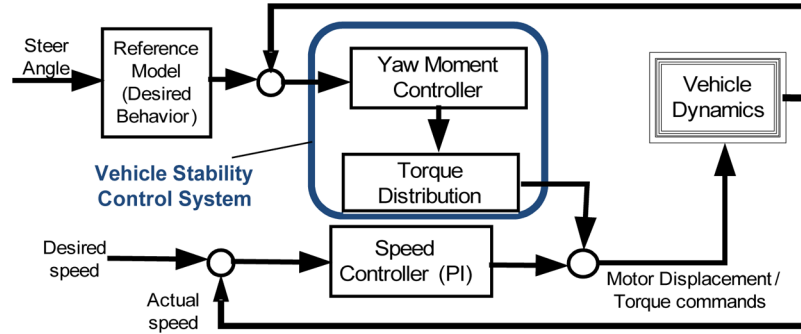
3.2   Vehicle stability control

The speed controller in Figure 6 represents the driver's intent of maintaining a desired forward speed for the vehicle. The motor displacement/torque commands from the speed controller serve to overcome resistance loads of aerodynamic drag, rolling resistance, and grade. The VSC system also modulates the individual torques of the wheel-end P/Ms to alter the vehicles handling and trajectory without seriously degrading the driver's intentions. This is achieved through a cascade of yaw moment control and a torque distribution strategy as shown in Figure 6. Several yaw moment controllers (yaw rate feedback, lateral acceleration feedback or combined feedback), and torque distribution strategies have been previously assessed for some strengths and weaknesses (Karogal and Ayalew, 2009; Osborn and Shim, 2004), though an ideal strategy has yet to be conclusively determined. In this paper, a simple 2 DOF steady-state handling response model is used to prescribe a desired vehicle behaviour, characterised by a yaw rate gain based on vehicle velocity and driver steering input. The discussion here is restricted to a yaw rate feedback stability controller (of a PID type), which compares the desired

yaw rate to the actual yaw rate of the vehicle to determine if the vehicle has excessive or insufficient yaw rate (over-steer or under-steer). If excessive yaw rate error is observed, the stability controller acts to reduce the yaw rate error by applying a corrective yaw moment defined by:

$$M_\psi = \left(K_p + \frac{K_I}{s} + K_D s \right)\left(\dot\psi_{\text{desired}} - \dot\psi \right) \tag{22}$$

where, $\dot\psi_{\text{desired}} = f(\delta, V)$ is determined from the steady state yaw rate response at the prevailing vehicle speed V. The torque distribution strategy then dictates how the corrective yaw moment is achieved by modulating the torque output of the individual wheel-end P/Ms via the respective displacement factors (see equation (2)). The distribution strategy applied in this work (form a total of 4 suggested in previous work (Karogal and Ayalew, 2009)) involves reducing the torque of the wheel-end P/Ms on the left or right sides of the vehicle to generate a positive or negative yaw moment.

Figure 6 Schematic of vehicle stability controller architecture (see online version for colours)

Given the above discussion, the wheel-end P/M torque commands have two components serving to maintain vehicle speed or stability control. For the front left motors, these are denoted by $x_{F,V}$ and $x_{LF,C}$ (which determines $M\psi$), respectively. For each motor, the speed control component is determined considering the drive split ratio for the drive train. Here all four motors are assumed to contribute equally. For the stability control component, a left-to-right side switch is activated based on yaw-rate error to generate the desired corrective moment. The following equations give the motor displacement factors adding the two components for the left and right front motors.

$$x_{m,\text{LF}} = \begin{cases} x_{F,V} + x_{\text{LF},C} & \left(\dot\psi_{\text{desired}} - \dot\psi\right) > 0 \\ x_{F,V} & \left(\dot\psi_{\text{desired}} - \dot\psi\right) < 0 \end{cases} \tag{23}$$

$$x_{m,\text{RF}} = \begin{cases} x_{F,V} & \left(\dot\psi_{\text{desired}} - \dot\psi\right) > 0 \\ x_{F,V} + x_{\text{RF},C} & \left(\dot\psi_{\text{desired}} - \dot\psi\right) < 0 \end{cases} \tag{24}$$

A final comment is in-order regarding the generation of the reference/desired yaw rate. The reference model used here is based on the steady-state gain from the bicycle model of the vehicle and computes the desired yaw rate from the steer angle input and the forward vehicle speed.

4   Results and discussions

The system model described in Section 2 along with the power management strategy described Section 3.1 were used to select component sizes and control threshold parameters for the independent hydrostatic drive system proposed in Figure 1, with the objective of improving fuel mileage and acceleration performance for a mid-size truck. The analysis started with the stock engine for a Ford F-150 truck (4.5 L, V-8, 172 kW SI engine) and considered that the upgraded powertrain with the independent hydrostatic drive to work with a larger truck with a GVW of 8000 lbs (about 20% heavier). In addition, the selection of the hydrostatic components was limited to stock components for which test data were available. The following components are the result of the iterative optimisation and component selection exercise: wheel-end P/M displacement of 55 cm^3/rev; engine mounted pump displacement of 125 cm^3/rev; gear ratio between the P/M and the wheel of 4.00; and high pressure and low pressure accumulator volumes of 20 gallon. Using these sets of component sizes, further fuel economy optimisation and safety considerations led to the following sets of parameters for the accumulator and engine operating thresholds: Pre-charge pressure = 13 MPa, Maximum pressure = 40 MPa, engine-off SOC threshold = 40%, SOC dead band = 10%, threshold engine power = 45 kW.

The vehicle considered was a nominally over-steering vehicle (a worst-case scenario) with font-rear distributions of 45–55% in weight, 45–55% in drive and 30–70% in roll stiffness, and on dry asphalt road ($\mu = 1.0$). While the side-to-side distribution of torque for the stability controller was determined via equations (23) and (24), for the front-rear split, a slightly front-biased distribution of 55–45% was considered for the stability control component in the results given below.

4.1   Closed loop performance

To evaluate the performance of the proposed system and its power management scheme in a handling manoeuvre, the system model was exercised in a swept sine steer test. Figure 7 shows the powertrain responses to a 3 deg road wheel angle steer input at a target forward speed of 80 kph. The power management scheme works as designed (Section 3.1) with the accumulator supplying the primary drive power as long as its SOC is above the engine-off threshold. Below the engine-on threshold SOC, the engine power output is increased beyond the nominal 45 kW until the SOC of the accumulator recovers. The displacement factors of the wheel-end P/Ms are manipulated by both the speed and stability controllers in response to the steer input. As the frequency increases, the accumulator takes up the main fluctuations in the demand power by frequent charging and discharging. This is a desirable attribute of the accumulator.

To further investigate the handling response in the frequency domain, the yaw rate and lateral acceleration transfer functions were computed through Fast Fourier Transforms (FFTs) from the responses to the steer input given above. The results are shown in Figure 8. It can be seen that the stability controller acts to increase the bandwidth of the yaw rate response and reduce the yaw rate and lateral acceleration phase lags (for the later, to frequencies of about 1.5 Hz). The present control structure seems to have little effect on the steady-state yaw-rate or lateral acceleration responses.

Figure 7 Controlled system response to a 3 deg swept-sine steer input with speed controlled at 80 kph (see online version for colours)
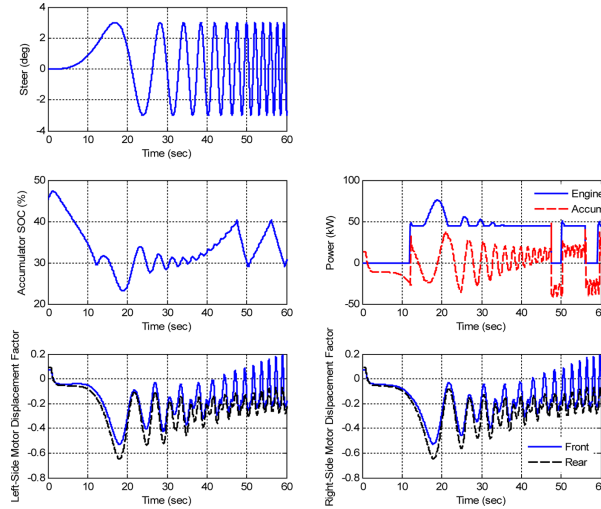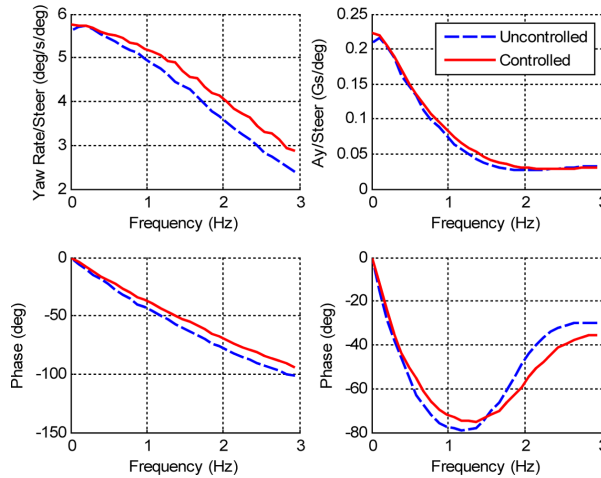

Figure 8 Controlled and uncontrolled vehicle yaw rate and lateral acceleration transfer functions (see online version for colours)


4.2 Stability and energy recovery

To evaluate the handling performance in aggressive manoeuvres, a 'sine with dwell' steering angle input was considered. This open-loop manoeuvre has been defined by NHTSA in the USA to emulate a severe obstacle avoidance type manoeuvre in evaluating VSC systems by inducing dynamic nonlinear vehicle responses (NHTSA, 2007). For the simulation results shown below, in-order to isolate the stabilising function of the proposed system, the driver's acceleration or braking input was set to zero during the evasive manoeuvre. That is, the speed control component was turned off after achieving the target speed of 80 kph just before the start of the manoeuvre. The vehicle responses with and without the stability controller during this manoeuvre are shown in Figure 9.

Figure 9   Controlled and uncontrolled vehicle handling performance in an evasive manoeuvre
(see online version for colours)
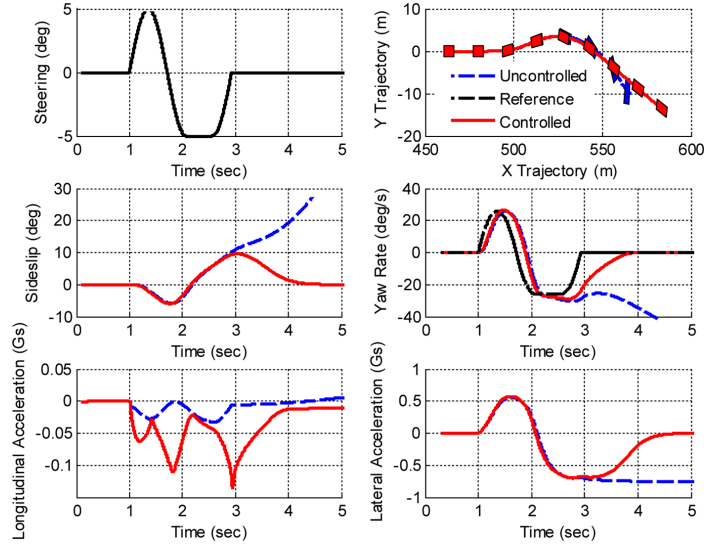
Clearly, the handling response of the vehicle with the controlled system shows significant improvement as compared to the uncontrolled response which exhibits unstable oversteer, excessive side-slip and yaw rate. It should be noted that the stabilising action will slow down the vehicle, as shown by the higher longitudinal deceleration magnitudes of the controlled vehicle response. This reduction in speed, from 80 kph to about 74 kph in the present case, can be considered an acceptable tradeoff for maintaining lateral handling stability. Furthermore, the stability controller uses entirely the wheel-end P/Ms to accomplish the course corrections without using the friction brakes. This exploits the energy recovery attributes of the hydrostatic powertrain. The performance of the hydrostatic powertrain during the same avoidance manoeuvre depicted in Figure 9 is detailed in Figure 10.

Figure 10   Performance of the hydrostatic powertrain during the stability controlled manoeuvre
(see online version for colours)
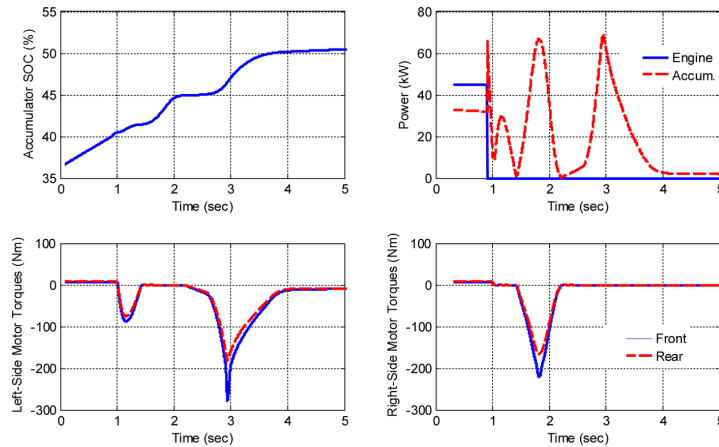
Unlike a traditional brake-based VSC system where energy is wasted as heat while accomplishing course corrections, this independent hydrostatic drive VSC system can recover energy (while generating the corrective yaw moment) by momentarily recharging the accumulator by the wheel-end P/Ms. Note that for this particular manoeuvre, the engine is turned off just before the start of the steer manoeuvre (top right plot in Figure 10). The power flow of the accumulator shows charging (positive power) when first, the left wheel-end P/M and then, the right wheel-end P/Ms and finally, the left wheel-end P/Ms are operated as pumps (negative torques). These results clearly show the potential of independent hydrostatic wheel drives for integrating regenerative braking for energy efficiency as well as torque distribution for VSC.

5 Conclusions and future work

In this paper, an independent hydrostatic wheel drive system has been considered from the point of view of enabling vehicle dynamics control in addition to energy recovery. A detailed causal forward-facing model of the proposed system has been outlined; including those of the hydrostatic system components (i.e., pump, wheel-end P/M, accumulators and transmission lines), the engine, the 7 DOF vehicle dynamics and a combined tyre-slip model suitable for the traction-based stability control. The supervisory controller includes an SOC-based power management scheme and a Vehicle Stability Control (VSC) strategy. With the latter, a corrective yaw moment is determined based on yaw rate feedback error and then a torque distribution strategy allocates the torque demand to each wheel-end pump/motor to generate the required corrective yaw moment.

The system model was used to analyse the handling performance of a mid-size truck, which was about 20% heavier than the baseline truck to take into account the upgraded capability and weight from added hydrostatic system components. Using simulations, it was shown how VSC schemes implemented with the independent hydrostatic drive system can include energy regeneration events within handling manoeuvres, thereby effectively integrating energy efficiency and vehicle safety functions. Further maintenance cost savings are possible from minimising the use of friction brakes to stabilise the vehicle during aggressive handling manoeuvres.

Further work on this topic will include: the improvement of the vehicle dynamics model to incorporate dynamic suspension effects (roll, pitch, heave), investigation of alternative yaw moment controllers (e.g., estimated side-slip angle and lateral acceleration feedback) and torque distribution strategies (progressive engagement based on degree of instability or weight transfer), and implementation of alternative power management strategies.

References

Ayalew, B. and Kulakowski, B.T. (2005) 'Modal approximation of distributed dynamics for a hydraulic transmission line with pressure input – flow rate output causality', *Transactions of the ASME, Journal of Dynamic Systems Measurement and Control*, Vol. 127, No. 3, pp.503–507.

Brahma, A., Guezennrc, Y. and Rizzoni, G. (2000) 'Optimal energy management in series hybrid electric vehicles', *Proceedings of the American Control Conference*, 28–30 June, Chicago, IL, pp.60–64.

Buchwald, P., Christensen, G., Larsen, H. and Pedersen, P.S. (1979) *Improvement of a Citybus Fuel Economy using a Hydraulic Hybrid Propulsion System – A Theoretical and Experimental Study*, SAE Paper No. 790305.

Cengel, Y.A. and Boles, M.A. (2005) *Thermodynamics: An Engineering Approach*, McGraw-Hill, New York.

Esmailzadeh, E., Goodarzi, A. and Vossoughi, G.R. (2002) 'Directional stability and control of four-wheel independent drive electric vehicles', *Proc. Instn. Mech. Engrs. Part K: Journal of Multi-body Dynamics*, Vol. 216, No. 4, pp.303–313.

Filipi, Z., Louca, L., Daran, B., Lin, C-V., Yildri, U., Wu, B., Kokkolaras, M., Assanis, D., Peng, H., Papalambros, P., Stein, J., Szukubiel, D. and Chapp, R. (2004) 'Combined optimization of design and power management of the hydraulic hybrid propulsion system for the 6×6 medium truck', *Int. J. Heavy Vehicle Systems*, Vol. 11, Nos. 3–4, pp.372–402.

Genta, G. (1997) *Motor Vehicle Dynamics: Modelling and Simulation*, World Scientific, Singapore.

Ghoneim, Y., Lin, W.C., Sidolsky, D.M., Chen, H.H., Chin, Y-K. and Tedrake, M.J. (2000) 'Integrated chassis control system to enhance vehicle stability', *International Journal of Vehicle Design*, Vol. 23, Nos. 1–2, pp.124–144.

Goodarzi, A. and Esmailzadeh, E. (2007) 'Design of a VDC system for all-wheel independent drive vehicles', *IEEE/ASME Transactions on Mechatronics*, Vol. 12, No. 6, pp.632–639.

Gradu, M. (2003) *Torque Bias Coupling for AWD Applications*, SAE Paper No. 2003-01-0676.

Jalil, N., Kheir, N.A. and Salman, M. (1997) 'A ruled-based energy management strategy for a series hybrid vehicle', *Proceedings of the American Control Conference*, June, Albuquerque, NM, pp.689–693.

Kargul, J.J. (2006) 'Hydraulic hyrbids: cost-effective clean urban vehicles', Presented at the *Michigan Clean Fleet Conference*, 22 March, Detroit, MI.

Karogal, I. and Ayalew, B. (2009) *Independent Torque Distribution Strategies for Vehicle Stability Control*, SAE World Congress and Exposition, Detroit, MI, Paper Number 2009-01-0456.

Kim, Y.J. and Filipi, Z. (2007) *Simulation Study of a Series Hydraulic Hybrid Propulsion System for a Light Truck*, SAE Paper Number 2007-01-4151.

Lin, C-C., Peng, H., Grizzle, J.W. and Kang, J-M. (2003) 'Power management strategy for a parallel hybrid electric truck', *IEEE Transactions on Control Systems Technology*, Vol. 11, No. 6, pp.839–849.

McCandlish, D. and Dorey, R.E. (1984) 'The mathematical modelling of hydrostatic pumps and motors', *Proceeding of Inst. Mech. Engineers. Part B.*, Vol. 198, No. 10, pp.165–174.

NHTSA (2007) *FMVSS 126 – Electronic Stability Control Systems; Controls and Displays; 49 CFR Parts 571 and 585*, US National Highway Traffic Safety Administration (NHTSA).

Osborn, R.P. and Shim, T. (2004) *Independent Control of All-Wheel-Drive Torque Distribution*, SAE Paper Number 2004-01-2052.

Pacejka, H.B. (2002) *Tyre and Vehicle Dynamics*, Butterworth-Heinemann, Oxford.

Pease, G. and Henderson, J.M. (1988) 'Simulation of a hydraulic hybrid vehicle using bond graphs', *Journal of Mechanisms, Transmissions, and Automation in Design*, Vol. 110, pp.365–369.

Piyabongkarn, D., Lew, J.Y., Rajamani, R., Grogg, J.A. and Yuan, Q. (2007) 'On the use of torque-biasing systems for electronic stability control: limitations and possibilities', *IEEE Transaction on Control Systems Technology*, Vol. 15, No. 3, pp.581–589.

Pourmovahed, A. (1990) 'An experimental thermal time constant correlation for hydraulic accumulators', *Transactions of ASME, Journal of Dynamic Systems, Measurement and Control*, Vol. 112, pp.116–121.

Pourmovahed, A. (1991) 'Vehicle propulsion systems with a hydraulic energy storage: a literature survey', *International Journal of Vehicle Design*, Vol. 12, No. 4, pp.378–403.

Pourmovahed, A., Beachley, N.H. and Fronczak, F.J. (1992) 'Modelling of a hydraulic energy regeneration system – part I: analytical treatment', *Transactions of ASME, Journal of Dynamic Systems, Measurement and Control*, Vol. 114, pp.155–159.

Rajamani, R. (2006) *Vehicle Dynamics and Control*, Springer Science, New York.

VanZanten, T. (2000) 'Bosch ESP systems: 5 years of experience', *SAE Automotive Dynamics & Stability Conference*, SAE Paper Number 2000-01-1633, May, Troy, MI.

Watton, J. (1989) *Fluid Power Systems: Modelling, Simulation, Analog and Microcomputer Control*, Prentice-Hall International Ltd., UK.

Wilson, W.E. (1946) 'Rotary-pump theory', *ASME Transactions*, Vol. 68, No. 4, pp.371–384.

Wu, B., Lin, C-C., Filipi, Z., Peng, H. and Assanis, D. (2004) 'Optimal power management for a hydraulic hybrid delivery truck', *Vehicle System Dynamics*, Vol. 42, pp.23–40.

Nomenclature

A	Vehicle frontal area
A_w	Effective accumulator wall area
C_D	Drag coefficient
c_f	Constant pressure specific heat of foam
c_v	Constant volume specific heat of gas
D	Maximum displacement of pump/motor
F_x	Longitudinal tyre force
F_y	Lateral tyre force
F_z	Normal tyre load
g	Gravitational constant
h	Heat transfer coefficient
h_{cg}	Vehicle C.G. height
h_{rcF}, h_{rcR}	Front/rear roll centre height
I_{zz}	Yaw inertia
I_w	Inertia of motor/wheel referred to wheel
J_{eq}	Equivalent inertia of the pump/engine
$K_{\phi R}, K_{\phi L}$	Rear/front roll stiffness
l	Wheel base
l_f, l_r	Distance of front/rear axle from vehicle C.G.
m	Total vehicle mass
m_f	Mass of foam in accumulator
m_g	Mass of the gas in accumulator
n	Number of wheel-end P/Ms
P_e	Engine power
p_g	Gas pressure
p_j	Junction pressure
p_p, p_m	Pump/motor pressure
Q_{acc}	Accumulator flow rate

Q_{ap}, Q_{am}	Actual pump/motor flow rate
Q_i	Ideal flow rate
R_w	Effective wheel radius
T_{ap}, T_{am}	Actual pump/motor torque
d_f, d_r	Front/rear wheel track width
T_a	Actual torque
T_L	Load torque
T_w	Accumulator wall temperature
V_x	Longitudinal velocity in vehicle x-axis
V_y	Lateral velocity in vehicle y-axis
v	Specific volume of the gas
x	Displacement factor for pump/motor
ω_{e_des}, $\omega_{e/p}$	Desired/actual rotational speed of the engine-pump
ω_i, or, ω_w	Rotational speed of wheel i
α_i	Lateral slip angle of tyre i
δ	Road wheel steering angle
ρ	Density of air
κ_i	Longitudinal slip of tyre i
$\dot{\psi}$	Vehicle yaw rate
τ	Thermal time constant
η_v	Volumetric efficiency
η_m	Mechanical efficiency
ΔP	Pressure difference across pump/motor